Engineering One-Signal Activated TILs with CD3ζ-CD28 Chimeras for Potent Antitumor Activity in Solid Tumors

Yongqiang Wu[1,2 † *], Xueshuai Ye[3†], Yufeng Zhu[1†], Shengchao Liu[4], Jiabao Song[4], Qichen Yuan[5], Dejing Kong[4], Lianmei Zhao[2*]

1. Gene Editing Research Center, Hebei University of Science and Technology, Shijiazhuang 050000, China.
2. Research Center, The Fourth Affiliated Hospital of Hebei Medical University, Shijiazhuang, Hebei, 050017, China;
3. The Affiliated HospitalandSchool of Clinical Medicine, Hebei University of Engineering, Handan, 056000, Hebei, China.
4. Collegeof Food Science and Biology, Hebei University of Science and Technology, Shijiazhuang 050000, China.
5. Department of Chemical and Biomolecular Engineering, Rice University,Houston, Texas, USA.

† These authors contributed equally to this work.

* Correspondence to wuyongqiang@hebust.edu.cn ; 48100996@hebmu.edu.cn;

Abstract

Adoptive T cell therapy (ACT) with autologous tumor-infiltrating lymphocytes (TILs) has shown robust anti-tumor efficacy in solid tumors, yet suboptimal stability and clinical outcomes remain critical challenges. Here, we introduce One-Signal-Activated TIL (OSAT), a novel engineering strategy that integrates CD3ζ with secondary signaling domains to bypass the classical dual-signal requirement for T cell activation. Among ten designed constructs, two OSAT molecules achieved efficient single-signal activation, recapitulating the activation signatures and functional markers of wild-type T cells under dual-signal stimulation. OSAT demonstrated potent in vitro cytotoxicity and in vivo anti-tumor activity across syngeneic models of melanoma and colorectal cancer, particularly when combined with PD-1 blockade. These findings establish OSAT as a promising therapeutic platform for overcoming TIL therapy limitations in solid tumors.

Keywords: Adoptive cell therapy, Tumor-infiltrating lymphocytes, CD3ζ, CD28, Solid tumors, One-signal activation

Introduction

The immune system plays a pivotal role in tumor immunosurveillance, and advances in cancer immunotherapy—including ACT[1-3] and immune checkpoint inhibitor (ICI)[4]—have revolutionized cancer treatment. Chimeric antigen receptor (CAR)-T cell therapy, particularly targeting CD19/CD20, has achieved landmark success in hematological malignancies[5]. However, translating CAR-T technology to solid tumors remains challenging due to antigen heterogeneity, immunosuppressive microenvironments, and limited tumor infiltration[6]. TIL therapy involves the isolation and purification of specific antitumor lymphocytes from solid tumor tissue, followed by their amplification and activation before administration. TILs can naturally target patient-specific tumor antigens and infiltrate tumor tissue to eliminate tumor cells through direct contact or cytokine release. This capability positions TILs as a promising solution to the challenge of recognizing tumor antigens in the context of solid tumor therapy[7-8].Nevertheless, TIL therapy still encounters

obstacles in treating solid tumors due to the diverse microenvironments and immune cell states present within these tumors.
T cell activation requires the simultaneous recognition of tumor cells expressing MHC class I molecules/antigenic peptides and antigen-presenting cells (APCs) that provide necessary stimulatory signals. T cells can only mount an effective immune response against cancer cells in the presence of APCs[9]. T cell activation requires dual signals: (1) TCR engagement with MHC/peptide complexes and (2) co-stimulation via CD28–CD80/86 interactions[10-11]. In the tumor microenvironment (TME), dysfunctional APCs often fail to provide adequate co-stimulation, leading to T cell anergy[12]. Moreover, sustained CD28 signaling is critical for maintaining TCF-1^{+} PD-1^{+} CD8^{+} T cell stemness and effector function[13]. TME is a complex ecosystem composed of tumor cells and surrounding cells, including various immune cells such as DCs, macrophages, and T cells, which interact to shape the immune status. APCs play a central role in TME by presenting tumor antigens and activating T cells[12]. However, native T cells may remain inactivated due to the absence of co-stimulatory signals from APCs, leading to immune tolerance[13]. Furthermore, sustained CD28 co-stimulation is essential for the self-renewal and differentiation of TCF-1^{+} PD-1^{+} CD8 T cells, as well as for maintaining the functionality of effector T cells[14]. Thus, stabilizing the provision of T cell co-stimulatory signals may be key to the success of TIL immunotherapy. In the 2006 TGN1412 phase I clinical trial involving CD28 monoclonal antibodies, six healthy male volunteers rapidly developed severe systemic inflammatory responses after receiving a single dose of the antibody, resulting in critical conditions[15]. This indicates that the sole use of CD28 monoclonal antibodies can have significant side effects, making it challenging to support TIL in combating tumors.

Here, we introduce the OSAT approach, designed to optimize the T cell activation process to enhance the antitumor efficacy of TILs. Our innovation involves the development of a single-step activation receptor that integrates essential intracellular co-stimulatory signals within TIL cells. Our findings demonstrate that the modified TIL cells can directly identify and eliminate tumor cells, bypassing the need for co-stimulatory signals from APCs. Importantly, these modified TILs retained their specific tumor recognition and tissue infiltration capabilities, and no significant inflammatory responses were observed in vivo. Furthermore, we validated the efficacy and safety of the modified TILs in combination with PD-1 blockade in mouse tumor models, resulting in robust antitumor activity. This study highlights a compelling therapeutic strategy that harnesses TILs and their synergistic interaction with immune checkpoint inhibitors for effectively combating malignant solid tumors.

Results

Overview of OSAT design and screening of OSAT molecules

T cell activation is a sequential process involving antigen recognition, signal transduction, transcriptional reprogramming, and effector enzyme activation[16]. Naïve T cell priming requires dual signals: TCR engagement with MHC-bound peptides and CD28 co-stimulation by APCs (Fig. 1a)[10-11,17]. In TME, immunosuppressive factors and regulatory immune cells often impair APC functionality—the sole cell subset capable of initiating primary T cell activation[18]. Concurrently, chronic TCR stimulation combined with insufficient CD28 signaling drives T cell exhaustion in TILs[13]. These aberrant signaling states culminate in T cell dysfunction, compromising anti-tumor immunity (Fig. 1b)[19-20].To address this, we engineered OSAT molecules consisting of chimeric CD3ζ cytoplasmic domains fused with costimulatory receptor intracellular domains (Fig. 1c). By covalently linking CD3ζ immunoreceptor tyrosine-based activation motifs (ITAMs) with signaling domains of CD28 or CD137, these constructs bypass APC dependency: upon TCR recognition of tumor-associated antigens, OSAT molecules mimic dual-signal activation, triggering robust T cell

cytotoxicity against tumor cells. This modular design aims to rejuvenate exhausted TILs and augment anti-tumor responses through streamlined yet robust signaling.

Building on the success of CAR-T cell therapy[1], which relies on CD3ζ ITAMs and CD28/CD137 costimulatory domains for B-cell malignancy treatment[2], we designed OSAT molecules by fusing full-length CD3ζ with CD28 and CD137 intracellular domains in combinatorial configurations (Fig. 1d; Supplementary File). To enable high-throughput screening, EF1α promoter-driven lentiviral vectors expressing CD3ζ-CD28/CD137 chimeras were constructed and transduced into Jurkat cells. Stable cell lines were established via puromycin selection (Fig. 1e). Activation profiles were evaluated by ELISA quantification of IL-2 secretion following anti-CD3 (OKT3) stimulation. Two constructs—M2 (CD3ζ-CD28) and M7 (CD3ζ-CD137-CD28)—displayed robust activation responses (Fig. 1f). Notably, despite the inclusion of CD137's TNFRSF domain, M7 did not exhibit significantly enhanced signaling compared to M2 ($P > 0.05$), indicating CD28 remains the principal costimulatory mediator (Fig. 1f). These candidates were selected for downstream validation.

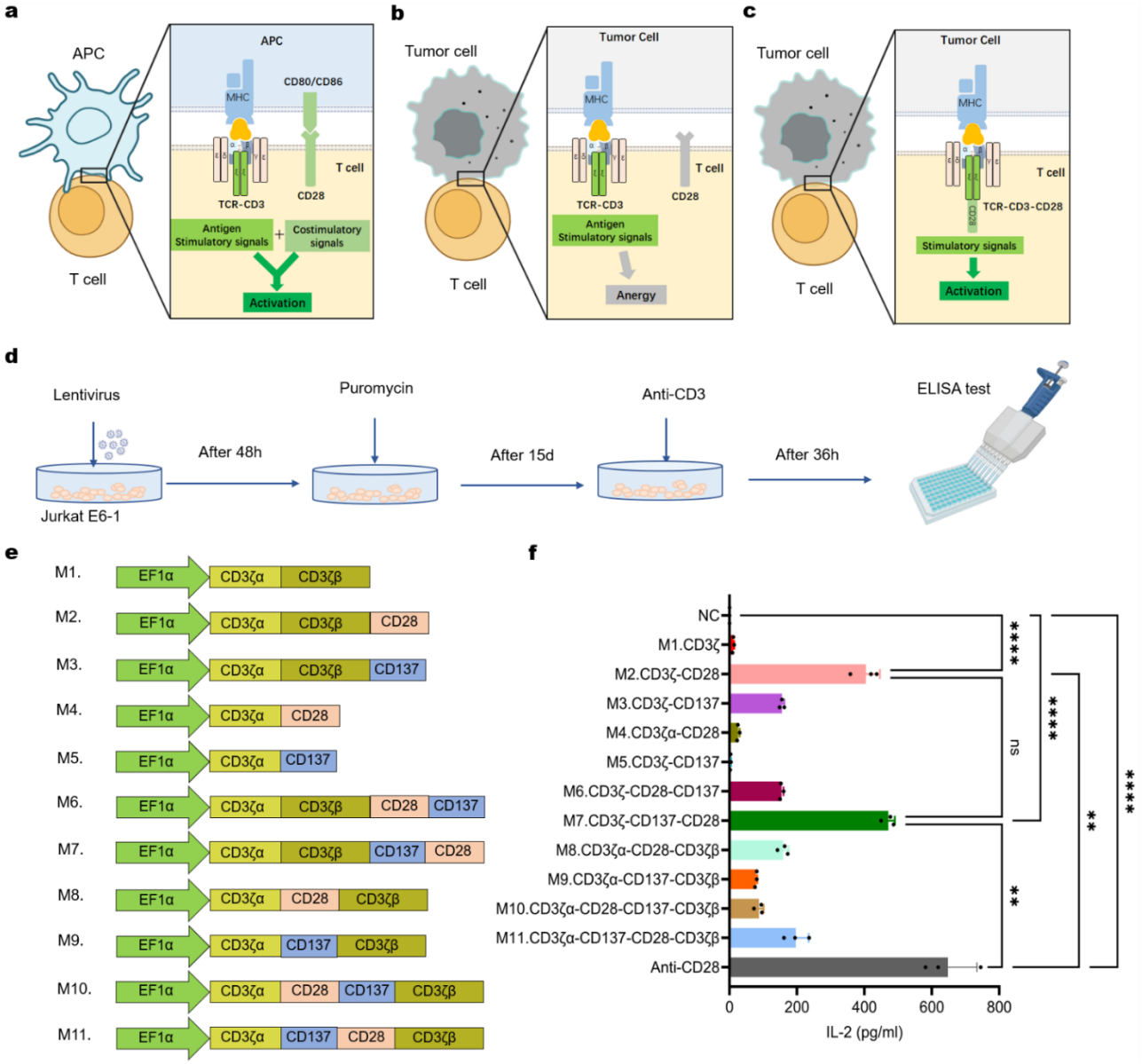

Fig.1 | Schematic representation of T cell activation mechanismsand screening of OSAT molecules

(a) Naïve T cell activation is dependent on dual-signal engagement: TCR recognition of MHC-presented antigenic peptides (Signal 1) and costimulatory receptor ligation (Signal 2) by professional APCs. **(b)** Unilateral TCR stimulation in the absence of costimulation induces T cell anergy and apoptotic cell death. In TME, this aberrant signaling promotes functional exhaustion of

TILs. **(c)** Hypothetical working model of OSAT: The chimeric construct integrates CD3ζ ITAMs with CD28 costimulatory domains, enabling antigen-independent T cell activation upon tumor cell contact. **(d)** High-throughput screening pipeline for OSAT molecules: Jurkat cells were transduced with lentiviral vectors expressing combinatorial CD3ζ-CD28/CD137 fusions, selected with 1 μg/mL puromycin, and activated with plate-bound anti-CD3 (OKT3). IL-2 secretion was quantified by ELISA to evaluate activation profiles. **(e)** Molecular architecture of OSAT constructs(CD3ζα: N-terminal extracellular/transmembrane domain (amino acids 1–51)，CD3ζβ: C-terminal ITAM-containing cytoplasmic domain (amino acids 52–163)，CD28: CD28 intracellular ITAM domain, CD137: CD137 intracellular ITAM domains). **(f)** Functional validation of OSAT constructs:Stably transfected JurkatE6-1 cells were stimulated with anti-CD3 (1 μg/mL). IL-2 concentrations were measured 24 h post-stimulation. Data represent mean ± SEM (n = 3 biologically independent experiments). Statistical significance was determined by one-way ANOVA with tukey's multiple comparisons test (*P < 0.05, **P < 0.01, ***P < 0.001, ****P <0.0001; ns = not significant).

Complete T cell activation mediated by OSAT molecules M2 and M7 under mono-signal stimulation

Dual-signal T cell activation via TCR engagement and costimulatory receptor engagement[18] initiates membrane depolarization, triggering Ca^{2+} release from the endoplasmic reticulum into the cytosol. Elevated cytosolic Ca^{2+} levels activate downstream signaling cascades, including the nuclear factor of activated T cells (NFAT) pathway, which coordinately enhances transcription factor activity (NF-κB, AP-1) critical for T cell proliferation, differentiation, and effector function programming (Fig. 2a)[20-21]. Therefore, intracellular Ca^{2+} dynamics and transcription factor activation serve as canonical markers of T cell activation status.

To characterize OSAT-mediated signaling, we leveraged Jurkat T cells—a tractable model system with reduced biological variability compared to primary cells[22]. Mono-signal anti-CD3 stimulation of OSA-Jurkat cells induced sustained Ca^{2+} flux comparable to dual-stimulated wild-type (WT) Jurkat cells (Fig. 2b). Phospho-protein analysis revealed significant upregulation of activated AP-1 and NF-κB in M2/M7 OSA-Jurkat cells 1 hour post-stimulation, whereas WT Jurkat cells showed no detectable activation under mono-signal conditions (Fig. 2c).

Transcriptomic profiling confirmed functional equivalence between OSA-Jurkat and dual-stimulated WT Jurkat cells. Principal component analysis (PCA) demonstrated high similarity in global gene expression patterns between OSA-Jurkat (mono-stimulated) and dual-stimulated WT Jurkat cells, while mono-stimulated WT Jurkat cells clustered separately (Fig. 2d). Venn analysis of differentially expressed genes (DEGs) identified ~30% overlap between OSA-Jurkat and dual-signal activation, with divergent enrichment in co-stimulatory and epigenetic regulatory pathways (Extended Data Fig. 1a). Hierarchical clustering revealed OSA-Jurkat cells activated under mono-signal conditions clustered closer to dual-stimulated WT Jurkat cells than to mono-stimulated WT controls (Fig. 2e). Functional annotation of DEGs highlighted upregulation of activation/effector genes (ICOS, IL2RA, GZMB) and metabolic reprogramming genes (MTPAP, HK2, PKM) in both dual-stimulated WT and M2-OSA Jurkat cells (Fig. 2f). Although M7-OSA Jurkat cells showed significant activation compared to unstimulated controls, they retained transcriptional differences relative to dual-stimulated WT cells(Fig. 2d-f). Gene Ontology (GO) enrichment analysis further validated signaling equivalence. Both dual-stimulated WT Jurkat cells (Extended Data Fig. 1b–d) and OSA-Jurkat cells displayed statistically significant enrichment of T cell activation-associated cellular components (CC), including immunological synapse formation and cytoskeletal remodeling ($P < 0.05$, Fisher's exact test). In contrast, mono-stimulated WT Jurkat cells showed no such enrichment (Extended Data Fig. 1e). These findings collectively demonstrate that OSAT molecules

recapitulate dual-signal activation programs under mono-signal conditions through combinatorial co-stimulatory signaling.

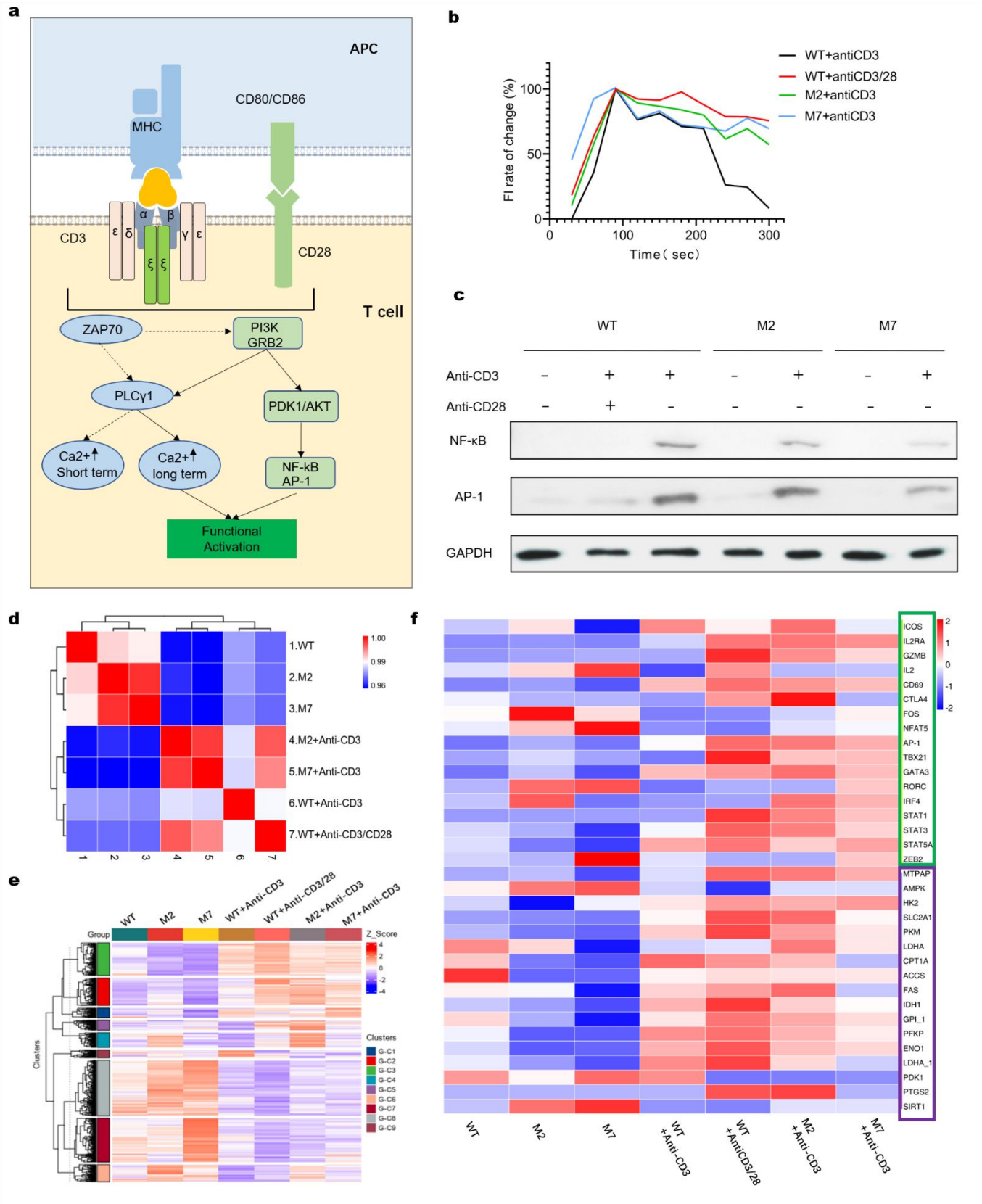

Fig. 2 |OSAT molecules recapitulate dual-signal activation programs under mono-signal stimulation

(a) Schematic representation of T cell activation signaling cascades. TCR engagement (Signal 1) and costimulatory receptor ligation (Signal 2) initiate PLCγ-mediated Ca^{2+} release from the endoplasmic reticulum, activating downstream transcription factors (NF-κB, AP-1) critical for effector programming. **(b)** Intracellular Ca^{2+} dynamics in Jurkat cells measured by Fura-8

AM-based calcium imaging following anti-CD3 (1 μg/mL) and/or anti-CD28 (1 μg/mL) stimulation. Data represent mean ± SEM (n = 3 biologically independent experiments). **(c)** Immunoblot analysis of phosphorylated transcription factors in Jurkat cells post-activation. Cells were stimulated with anti-CD3/CD28 for 60 minutes and probed with antibodies against phospho-NF-κB p65 (Ser536) and phospho-AP-1 c-Jun (Ser63). GAPDH served as a loading control. **(d)** Principal component analysis of global gene expression profiles in WT-Jurkat vs. OSA-Jurkat cells. Cells were stimulated for 12 hours, and transcriptomic data were normalized using Z-score transformation. **(e)** Heatmap of differentially expressed gene clusters of CD3 activations. Clusters highlight distinct transcriptional responses to mono- vs. dual-signal stimulation (Clustering was determined using k-means). **(f)** Heatmap of Z-score normalized expression for T cell activation markers (green) and metabolic pathway genes (purple) in OSA-Jurkat and WT Jurkat cells 12 hours post-stimulation.

Strategy for Stable and High-Efficiency OSATMoleculesExpression in T Cells

To enable OSA-mediated modification of TILs for tumor eradication, a safe, efficient, and rapid gene delivery method is critical. Established gene transfer approaches include CRISPR-Cas9-mediated gene editing, lentiviral transduction, and electroplasmid transfection[21-22]. The Cas9-HITI gene editing method[23] precisely inserts the OSA sequence into theCD3ζ locus while knocking out wild-typeCD3ζ, minimizing competition between endogenous CD3ζ and OSAT molecules (Fig. 3a). We initially evaluated multiple single-guide RNAs (sgRNAs) targeting theCD3ζ locus and identified the most effective sgRNA via T7E1 analysis (Extended Data Fig. 2a,b). Using this sgRNA, we designed an OSA-donor vector(incorporated a 2A-GFP cassette into the C-terminus) and co-transfected Jurkat cells with Cas9-sgRNA and OSA-Donor via electroporation. However, 72 hours post-transfection, the editing efficiency with the optimal sgRNA remained low at about 14% (Fig. 3c). For lentiviral transduction, we also incorporated a 2A-GFP cassette into the C-terminus of the OSAT construct to facilitate flow cytometry-based efficiency assessment (Fig. 3b). Lentiviral particles were produced and used to transduce Jurkat cells, yielding a transduction efficiency of about 64% at 72 hours (Fig. 3c). OSA expression levels were significantly higher compared to the gene-editing approach. To explore transient high-level expression, we employed a self-replicating plasmid with S/MAR ori[24]. This plasmid, featuring an EF1α promoter and S/MAR sequence (Supplementary File), achieved OSA expression rates of 69% at 72 hours post-transfection (Fig. 3c). Long-term stability analysis revealed that gene editing and lentiviral methods maintained stable OSA expression over two weeks, whereas electroplasmid transfection showed reduced expression (Extended Data Fig. 2c-e). All methods demonstrated comparable effects on Tcell proliferation (Fig. 3d). These results indicate that lentiviral transduction offers superior stable expression efficiency, while electroplasmid transfection provides transient high-level expression.

Engineering Primary T Cells with OSAT Molecules Achieves Co-StimulationIndependent Cytotoxicity and Cytokine Production

To evaluate OSAT functionality in primary T cells, we transduced M2/M7 constructs into human primary T cells using lentiviral vectors and performed functional assays under monoclonal antibody stimulation. Flow cytometry analysis showed minimal CD25/CD69 expression in unstimulated or anti-CD3activatedWTT cells. In contrast, OSA-engineered T cells displayed robust CD25/CD69 upregulation following anti-CD3 stimulation alone, with activation levels comparable to dual-stimulated WT T cells (Fig. 3e). Cytokine secretion profiles (IL-2, IFN-γ, TNF-α) demonstrated significant increases in all activated groups relative to controls, with no statistically significant differences between M2-OSA-mediated and dual-signal activation (Fig. 3f).

Functional validation utilized a cytotoxicity platform with 293T/MDA cells engineered to express CD3-specific ScFV on their surface. WT T cells required CD28 co-stimulation for consistent target cell killing (Fig. 3g), whereas OSA-modified T cells exhibited potent cytotoxicity without CD28 engagement (Fig. 3h). These results confirm that OSAT molecules fully activate primary T cells through TCR/CD3 engagement alone, bypassing traditional co- stimulation requirements while retaining cytotoxic effector functions. The observed CD25/CD69 upregulation aligns with established T-cell activation markers, validating OSAT ability to recapitulate dual-signal responses in cytotoxicity assays.

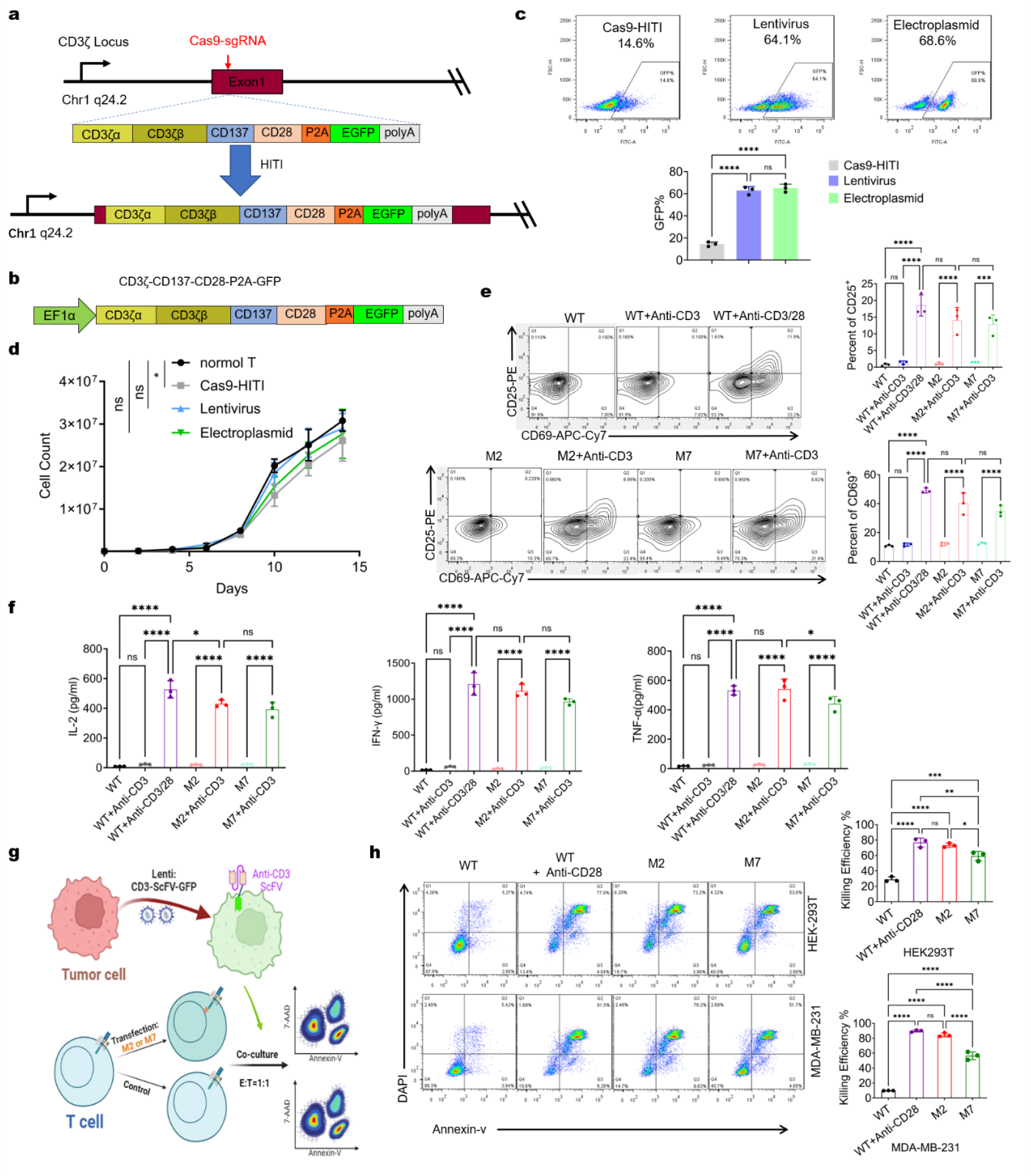

Fig. 3 |Functional Validation of OSAT Molecule Efficacy in Primary Human T Cells

(a) CRISPR-Cas9/HITI-mediated integration of the OSA gene and reporter gene (eGFP) into the CD3ζlocus. **(b)** Schematic representation of the OSATmolecules construct and reporter gene architecture in lentiviral vectors or self-replicating plasmids. **(c)** Flow cytometry analysis of OSA expression efficiency 72 hours post-transduction.Top: Representative flow plots showing OSA expression in primary T cells under indicated conditions.Bottom: Quantification of OSA-positive cell populations across three independent experiments. **(d)** Proliferation curves of unmodified T cells, lentivirus-transduced OSA-T cells, Cas9/HITI-engineered OSA-T cells, and electroporated control T cells. Data pooled from three donors. **(e)** T cell activation profiling. Left: Flow cytometry gating for CD25 and CD69 expression under specified stimulation conditions. Right: Quantification of CD25+/CD69+ populations across triplicate experiments. **(f)** Cytokine secretion profiles measured by ELISA. IL-2, IFN-γ, and TNF-α concentrations in supernatants following gene transfer and stimulation under indicated conditions. **(g)** Experimental workflow for assessing OSA-T cell cytotoxic activity mediated solely by primary (CD3) signaling. **(h)** Cytotoxic efficacy of primary T cells against HEK293T and MDA-MB-231 cell lines. Killing efficiency (%) was evaluated using a dual-marker（Annexin-VandDAPI） flow cytometry assay combined with quantitative analysis. All graphs represent triplicate experiments (n = 3 donors). Error bars denote mean ± SEM. Statistical significance was assessed by one-way ANOVA with tukey's multiple comparisons test for c-f and h (*P < 0.05, **P < 0.01, ***P < 0.001, ****P <0.0001; ns = not significant).

In Vitro Antitumor Activity of OSAT

To validate the in vivo antitumor efficacy of OSAT, we established subcutaneous murine tumor models. To ensure functional compatibility in murine systems, human OSATmoleculessequences were substituted with murine orthologs and evaluated in the EL-4 murine T cell line. Following electroporation with OSAT molecules or negative control (NC)-plasmid, cells were stimulated with anti-mouse CD3 monoclonal antibody 72 hours later. OSA-modified EL-4 cells demonstrated significantly elevated IL-2 and IFN-γ secretion compared to wild-type cells, which showed no IL-2 and IFN-γ induction (Fig. 4a,b), confirming functional conservation of OSAT molecules across species.Subcutaneous tumor models using B16, MC38, and TC-1 cell lines were generated to assess OSAT functionality. Upon reaching ~0.5 cm^3 tumor volume, $CD3^+$ TILs were isolated from dissociated tumors via magnetic-activated cell sorting (Fig. 4c) and transfected with OSA constructs. Co-culture assays with autologous tumor cells at varying effector-to-target (E:T) ratios revealed significantly enhanced cytotoxicity by OSAT compared to non-modified TILs across all tested ratios (Fig. 4d). In contrast, PBMC-derived $CD3^+$ T cells showed no tumor-specific killing activity, confirming TILs' intrinsic targeting specificity (Fig. 4d-e). ELISA analysis further demonstrated 2.3-to 4.1-fold higher IL-2 and IFN-γ secretion from OSAT at a 20:1 E:T ratio compared to controls (Fig. 4e). Collectively, these results indicate that OSA modification potentiates murine TILs' antitumor capacity through dual mechanisms of augmented cytotoxic activity and cytokine-mediated immune modulation.

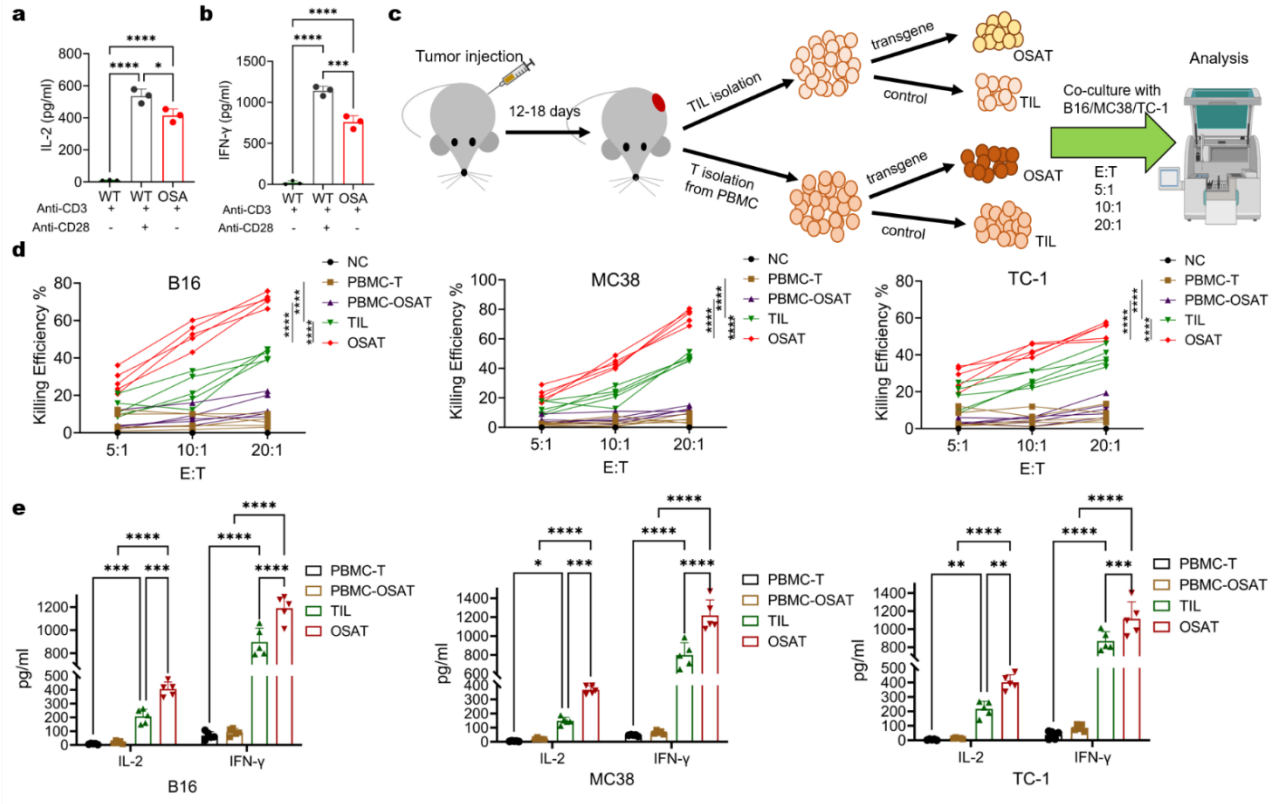

Fig. 4 |Functional evaluation of OSAT in vitro

(a-b) Cytokine production analysis of IL-2 and IFN-γ in EL-4 mouse T cells by ELISA. **(c)** Schematic representation of the experimental design for in vitro functional assessment of OSAT. **(d)** Dose-dependent cytotoxic activity of OSAT against B16, MC38, and TC-1 tumor cells at effector-to-target (E:T) ratios of 5:1, 10:1, and 20:1. **(e)** Cytokine secretion profiles (IL-2 and IFN-γ) measured by ELISA at a 20:1 E:T ratio across B16, MC38, and TC-1 tumor models. All graphs represent triplicate experiments (n = 3 donors). Error bars denote mean ± SEM. Statistical significance was assessed by one-way ANOVA(a and b) or two-way ANOVA (d and e) with tukey's multiple comparisons test. (*P < 0.05, **P < 0.01, ***P < 0.001, ****P <0.0001; ns = not significant).

In Vivo Superior Anti-Tumor Efficacy of OSAT

To investigate the in vivo antitumor activity of OSAT compared to traditional TILs, we established syngeneic B16, MC38, and TC-1 tumor models in mice, evaluating both therapeutic efficacy and safety (Fig. 5a). Given the prolonged treatment timeline required for in vivo studies, we first validated the sustained expression kinetics of lentiviral-delivered OSA-GFP over 14 days (Extended Fig. 3). The satisfactory results from this preliminary experiment confirmed that lentiviral vectors could maintain consistent transgene expression, which was critical for the long-term in vivo therapeutic effects. As a result, lentiviral vectors were selected as the optimal tool for in vivo OSA transduction. We conducted comprehensive antitumor efficacy assessments in all three syngeneic murine tumor models. In each model, OSAT consistently demonstrated superior antitumor efficacy compared to traditional TILs. Notably, in the MC38 model, OSAT exhibited significantly enhanced therapeutic efficacy compared to naive TILs (Fig. 5b). At 20 days post-treatment, tumors harvested from OSAT recipients were significantly smaller than those from n-TIL groups (Fig. 5c; Extended Fig. 4a). Survival analysis further revealed prolonged survival in OSAT-treated mice compared to traditional TIL groups (Fig. 5d).

Body weight monitoring showed no significant differences between treatment groups and controls throughout the study (Fig. 5e; Extended Fig. 4b,i). Safety evaluation focused on CRS risk through IL-6 and TNF-α serum profiling at 48 hours and 14 days post-treatment. Both TIL and OSAT groups

displayed significantly elevated cytokine levels compared to PBS controls at 48 hours, with OSATshowing higher levels (Fig. 5f-g; Extended Fig. 4c-d,j-k). Notably, in the TC-1 model,OSAT-treated mice exhibited slight body weight gain compared to controls, likely reflecting reduced tumor burden(Extended Fig. 4i). Hepatic and renal function markers (AST, ALT, NGAL, MCP-1) showed no significant differences between groups (Fig. 5 h-k; Extended Fig. 4e-h, l-o). Collectively, these results demonstrate that OSAT achieve enhanced tumor control and survival benefits compared to traditional TIL therapy while maintaining acceptable safety profiles.

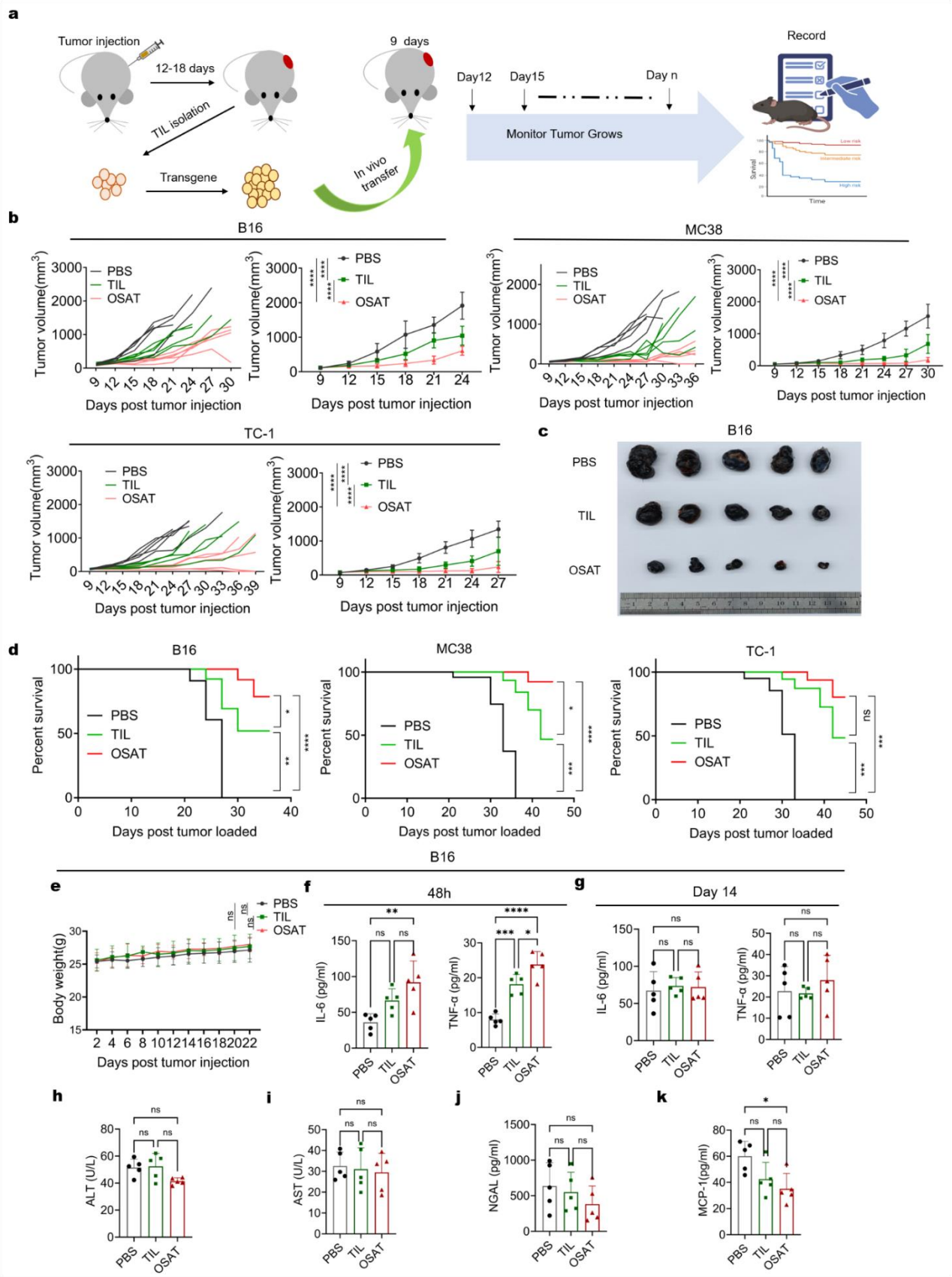

Fig. 5 |In vivo anti-tumor efficacy evaluation of OSAT in multiple tumor models

(a) Schematics of experimental design for adoptive transfer treatment in mouse models. **(b)** Tumor growth curves(individuals and groups) of B16/MC38/TC-1 that implanted subcutaneously and subjected to the indicated treatments. **(c)** Photographic images of representative B16 tumors in different groups on day 21 post tumor challenge (n = 5).Representative macroscopic images of excised B16 tumors across treatment groups at endpoint (tumors harvested on Day 21 post-inoculation; n = 5). **(d)** Kaplan-Meier survival curves for B16/MC38/TC-1 tumor-bearing mice treated with PBS, natural tumor-infiltrating lymphocytes (natural-TIL), or OSAT.**(e)**Body weight changes in B16 tumor-bearing mice across treatment groups (time-matched with tumor growth monitoring). **(f-g)** ELISA analysis of the cytokine production ofIL-6 and TNF-α in the sera of B16 model micethat subjected to the indicated treatment after 48hours or 14days.Statistical analysis was performed using non-parametric tests.（**h-k**）Serum biomarkers of hepatic toxicity (ALT, AST) and kidney toxicity (NGAL, MCP-1) at Day 14 post-treatment in the B16 model.The error bars indicatethe mean ± the standard error of the mean. Statistical significance was assessed by two-way ANOVA (band e),by one-way ANOVA(f-k),or by a log rank Mendel–Cox test (d).Each data point indicates an independent donor (n = 5). *P < 0.05, **P < 0.01, ***P < 0.001, ****P <0.0001; ns = not significant.

Enhanced Antitumor Efficacy of OSAT Combined with PD-1 Blockade Therapy

Following 12 days of OSAT treatment, tumors in B16 and MC38 models demonstrated rapid regrowth, particularly in the B16 model (Fig. 5b). We hypothesized that TILs might progressively upregulate immunosuppressive molecules, attenuating their antitumor activity. Flow cytometry analysis of immune checkpoint molecules (PD-1, TIM-3, LAG-3) in wild-type TILs isolated from B16 tumors at baseline (day 9) and post-treatment revealed a significant surge in PD-1 expression post-therapy, escalating from <10% at baseline to ~60% in the OSAT group (Fig. 6a). TIM-3 and LAG-3showed marginal increases with limited dynamic range (Fig. 6a). These findings suggested that combiningOSAT with PD-1 blockade could enhance therapeutic outcomes.

In vivo evaluation of OSAT plus PD-1 blockade (Fig. 6b) demonstrated sustained tumor suppression in the B16 model (Fig. 6c). All treatment groups outperformed PD-1 monotherapy in survival analysis, with the OSAT cohort achieving 100% survival at day 42 (Fig. 6d). Body weight monitoring confirmed minimal systemic toxicity across groups (Fig. 6e). Serum cytokine profiling at 48 hours and 14 days post-treatment revealed elevated IL-6 and TNF-α levels in both TIL and OSAT groups compared to PBS controls at 48 hours, confirming TIL activation (Fig. 6f-g). OSAT-treated mice exhibited higher IL-6 (170 pg/mL) and TNF-α (40 pg/mL) levels than conventional TILs, indicating enhanced functional activity. These elevations remained within safe thresholds. Hepatic and renal function markers (ALT, AST, NGAL, MCP-1) showed no significant differences between groups at day 14, confirming acceptable safety (Extended Fig. 5a-d). Collectively, OSAT therapy synergizes with PD-1 checkpoint inhibition to amplify antitumor efficacy while maintaining safety. This combinatorial approach represents a promising strategy to overcome TIL exhaustion and achieve durable tumor control.

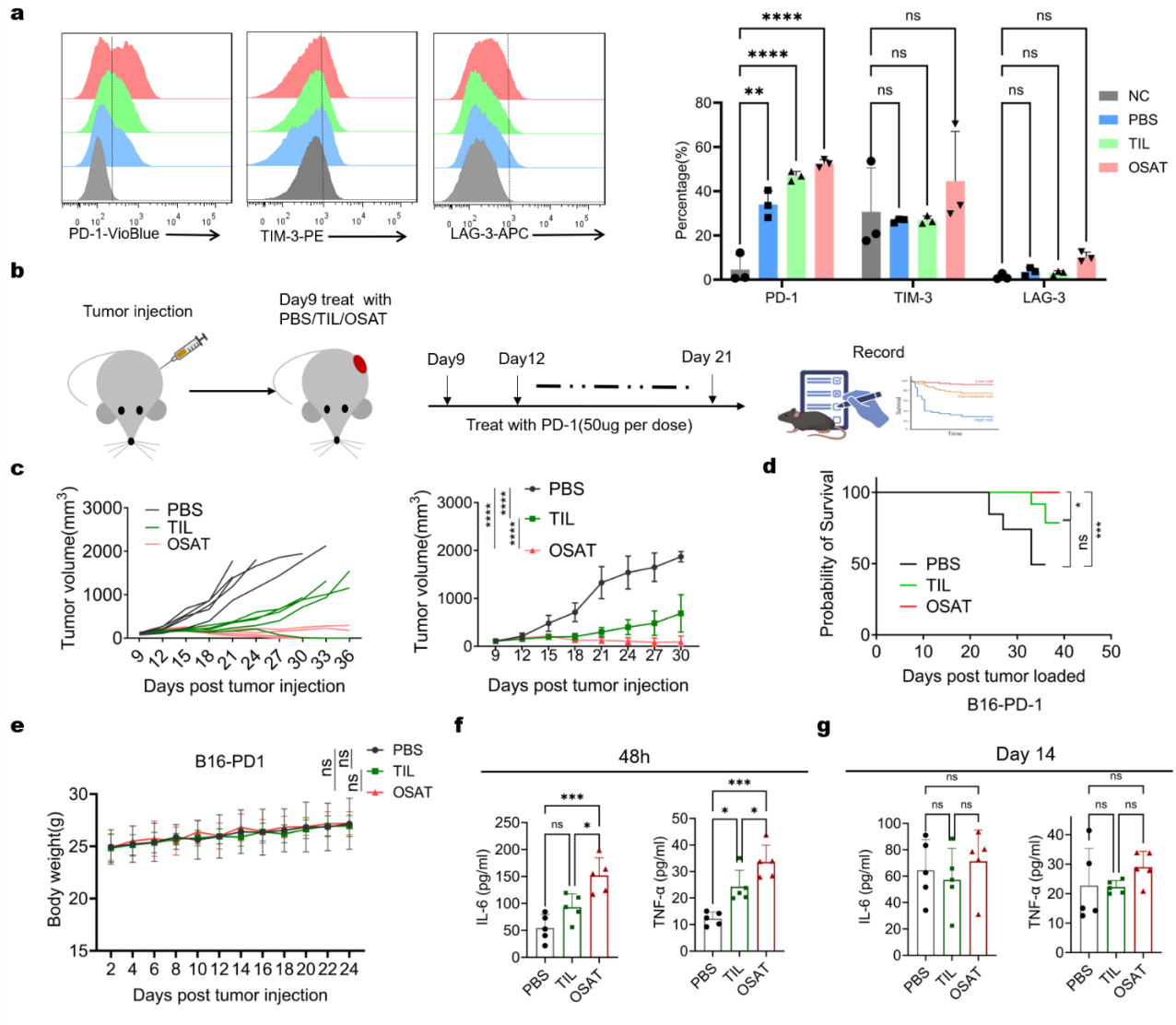

Fig. 6 |PD-1 blockade can further enhance in vivo anti-tumor activity of OSAT

(a) Comparison of the expression levels of PD-1, TIM-3, and LAG-3 in cells before and 12 days after treatment. Cells were classified into groups using flow cytometry. **(b)** Schematic illustration of the treatment strategy combining tumor-infiltrating lymphocytes (TIL) with PD-1 blockade.**(c)** Tumor growth curves (individual and group data) of the B16 tumor model mice that received PD-1 blockade and were subjected to the indicated treatments. **(d)** Percent survival curve of B16 tumor-bearing mice that received PD-1 blockade and were subjected to the indicated treatments. **(e)** Body weight changes in the B16 tumor model mice that received PD-1 blockade across different treatment groups (time-matched with the tumor growth monitoring period). **(f-g)** ELISA analysis of the cytokine production of IL-6 and TNF-α in the sera of B16 tumor model mice that received PD-1 blockade and were subjected to the indicated treatments. The analysis was conducted 48 hours or 14 days after treatment. Error bars represent mean ± standard error of the mean (SEM). Statistical significance was assessed bytwo-way ANOVA(a, c, and e),by log-rank (Mantel–Cox) test (d) and by one-way ANOVA(f and g) (*P < 0.05, **P < 0.01, ***P < 0.001, ****P <0.0001; ns = not significant.)

Discussion

This study provides experimental validation for the hypothesis that engineering TILs to rely on a single co-stimulatory activation signal can achieve potent antitumor activity. Our data demonstrate that fusing the CD3ζ and CD28 intracellular domains bypasses the traditional dual-signaling

requirement. The OSAT construct, upon single-signal activation, recapitulates gene expression profiles and functional markers comparable to wild-type T cells undergoing dual-signal activation[25]. Transcriptomic analysis revealed significant overlap between the OSAT single-signal activation signature and the dual-signal signature of wild-type T cells. Surface marker expression (CD25, CD69) reached equivalent levels, indicating that a single integrated signal suffices to drive full T cell activation. In vitro and in vivo experiments demonstrated that OSAT effectively inhibited tumor growth in multiple syngeneic models, including melanoma and colorectal cancer. Notably, combining OSAT with PD-1 blockade further enhanced therapeutic efficacy, confirming the robustness and clinical translational potential of this approach.

OSAT challenges the classical dual-signal theory of T cell activation while establishing the feasibility of single-signal activation through functional equivalence and broad antitumor activity across cancer types[25]. By engineering a synthetic signaling domain, we demonstrate that a single integrated signal can substitute for canonical co-stimulation. This aligns with emerging strategies exploring single-signal activation via synthetic receptor design[26], but uniquely focuses on native TCR diversity in TILs for solid tumor targeting. While prior studies have optimized signaling domains in CAR-T cells[27-28], our work pioneers the application of single-signal activation to TILs. The inherent tumor-specific heterogeneity and homing capabilities of TILs likely contribute to the observed therapeutic advantages. Evidence suggests that low-affinity T cells drive antitumor responses in humans and mice[29], and OSA modification may preferentially expand these populations, potentiating long-term efficacy. However, single-signal activation has been linked to T cell exhaustion[30-31]. Our combinatorial approach with PD-1 blockade mitigated this effect, highlighting the need for microenvironment modulation in engineered T cell strategies. The long-term persistence of single-signal activated T cells warrants further investigation. Despite isolation and $CD3^+$ enrichment, TILs retain functional heterogeneity[32]. Notably, while OSAT bypasses canonical dual signaling through engineered intracellular domains, a recent study describes a natural two-stage priming process for CD8 T cells, where CXCR3-mediated localization to IL-2-rich niches and CD4-derived paracrine IL-2 drive affinity-based clonal selection—both frameworks emphasize integrating key signaling pathways (synthetic domains vs. endogenous chemokine receptors) to optimize activation, proliferation, and functional differentiation for enhanced T cell efficacy[33].

Future research should identify T cell subsets most responsive to OSA modification and determine whether OSAT reduces inter-patient variability. The molecular mechanisms underlying resistance to exhaustion (e.g., epigenetic reprogramming) remain undefined. While validated in primary human T cells and immunocompetent murine models, our study lacks humanized tumor microenvironment models. Future studies will expand validation to additional tumor types (e.g., pancreatic cancer, glioblastoma) and patient-derived xenografts (PDX).

In summary, this work introduces a novel engineering strategy for TILs, generating single-signal activated TILs with enhanced antitumor activity in preclinical models. This approach addresses critical limitations in current TIL therapy and may facilitate broader application in solid tumor treatment.

References

1. Olson, D.J. &Odunsi, K. Adoptive cell therapy for nonhematologic solid tumors. *J Clin Oncol.* 2023;41(33):3397-3407.
2. Creelan, B.C. et al. Tumor-infiltrating lymphocyte treatment for anti-PD-1-resistant metastatic lung cancer: a phase 1 trial. *Nat Med.* 2021;27(8):1410-1418.

3. Norberg, S.M. & Hinrichs, C.S. Engineered T cell therapy for viral and non-viral epithelial cancers. *Cancer Cell.* 2023;41(1):58-69.
4. Bagchi, S., Yuan, R. &Engleman, E.G. Immune checkpoint inhibitors for the treatment of cancer: clinical impact and mechanisms of response and resistance. *Annu Rev Pathol.* 2021;16:223-249.
5. Brudno, J.N. &Kochenderfer, J.N. Chimeric antigen receptor T-cell therapies for lymphoma. *Nat Rev Clin Oncol.* 2018;15(1):31-46.
6. Maalej, K.M. et al. CAR-cell therapy in the era of solid tumor treatment: current challenges and emerging therapeutic advances. *Mol Cancer.* 2023;22(1):20.
7. Betof Warner, A., Corrie, P.G. & Hamid, O. Tumor-Infiltrating Lymphocyte Therapy in Melanoma: Facts to the Future. *Clin Cancer Res.* 2023;29(9):1835-1854.
8. Monberg, T.J. et al. TIL Therapy: Facts and Hopes. *Clin Cancer Res.* 2023;29(16):3275-3283.
9. Espinosa-Carrasco, G. et al. Intratumoral immune triads are required for immunotherapy-mediated elimination of solid tumors. *Cancer Cell.* 2024;42(7):1202-1216.e8.
10. Pittet, M.J. et al. Dendritic cells as shepherds of T cell immunity in cancer. *Immunity.* 2023;56(10):2218-2230.
11. Lotze, M.T. et al. CD28 co-stimulation: novel insights and applications in cancer immunotherapy. *Nat Rev Immunol.* 2024;24(12):878-895.
12. Elewaut, A. et al. Cancer cells impair monocyte-mediated T cell stimulation to evade immunity. *Nature.* 2025;637(8046):716-725.
13. Duraiswamy, J. et al. Myeloid antigen-presenting cell niches sustain antitumor T cells and license PD-1 blockade via CD28 costimulation. *Cancer Cell.* 2021;39(12):1623-1642.e1620.
14. Humblin, E. et al. Sustained CD28 costimulation is required for self-renewal and differentiation of TCF-1+ PD-1+ CD8 T cells. *Sci Immunol.* 2023;8(86):eadg0878.
15. Suntharalingam, G. et al. Cytokine storm in a phase 1 trial of the anti-CD28 monoclonal antibody TGN1412. *N Engl J Med.* 2006;355(10):1018-1028.
16. Obenauf, A.C. et al. Cancer cells impair monocyte-mediated T cell stimulation to evade immunity. *Nature.* 2025;631(7596):601-608.
17. Zagorulya, M., Duong, E. &Spranger, S. Impact of anatomic site on antigen-presenting cells in cancer. *J Immunother Cancer.* 2020;8(1):e000773.
18. Koch, M. et al. Dynamic regulation of CD28 conformation and signaling by charged lipids and ions. *Nat Immunol.* 2023;24(1):115-126.
19. de Janus, W.A. et al. Calcium signaling in T cells and its implications for immunotherapy. *Nat Rev Immunol.* 2010;10(8):564-576.
20. Thome, J.J. et al. The dual role of NFAT in T cell signaling. *Nat Immunol.* 2016;17(11):1534-1545.
21. Suzuki, K. et al. In vivo genome editing via CRISPR/Cas9-mediated homology-independent targeted integration. *Nature.* 2016;540(7632):144-149.
22. Bozza, M. et al. A nonviral, nonintegrating DNA nanovector platform for the safe, rapid, and persistent manufacture of recombinant T cells. *Sci Adv.* 2021;7(35):eabg2395.

23. June, C.H. et al. CAR T cell immunotherapy for human cancer. *Science.* 2018;359(6382):1361-1365.
24. Weiner, G.J. Building better monoclonal antibody-based therapeutics. *Nat Rev Cancer.* 2015;15(6):361-370.
25. Bretscher, P. & Cohn, M. A theory of self-nonself discrimination. *Science.* 1970;169(3947):1042-1049.
26. Smith, J.R. et al. Synthetic receptor design for single-signal activation. *Nat Immunol.* 2021;22(5):678-685.
27. Guedan, S. et al. Engineering T cell receptors with enhanced sensitivity and specificity for cancer immunotherapy. *Nat Immunol.* 2018;19(11):1253-1263.
28. Smith, J.M. et al. Single-signal activation of engineered T cells via synthetic co-stimulatory receptors. *Nat Biomed Eng.* 2021;5(8):781-792.
29. Gattinoni, L. et al. Low-avidity T cells drive endogenous tumor immunity in mice and humans. *Nat Immunol.* 2020;21(10):1195-1204.
30. Long, A.H. et al. 4-1BB costimulation ameliorates T cell exhaustion induced by tonic signaling of chimeric antigen receptors. *Nat Med.* 2015;21(5):581-590.
31. Tirosh, I. et al. Single-cell transcriptomic analysis of primary and metastatic tumor ecosystems in head and neck cancer. *Cell.* 2017;171(7):1611-1624.
32. Neftel, C. et al. An integrative model of cellular states, plasticity, and genetic vulnerability in glioblastoma. *Cell.* 2019;178(4):835-849.e21.
33. Jobin K. et al. A distinct priming phase regulates CD8 T cell immunity by orchestrating paracrine IL-2 signals. Science. 2025;388(6743):eadq1405.

Methods

Generation of OSA constructs

DNA fragments encoding human/mouse CD3ζ, CD28, and CD137 were chemically synthesized (Sangon Biotech). Fragments were cloned into pLVX-puro (Clontech) for lentiviral packaging using Gibson assembly[34]. Linearized/dephosphorylated vectors and PCR-amplified inserts were assembled following standard protocols. OSA fragments were also TA-cloned into pGEM-T Easy (Promega) for gene-editing donor use and ligated into modified pMC plasmids containing the APOB 3' MAR element[22]. The CMV promoter was replaced with the human EF1α promoter (amplified from genomic DNA). Final constructs were validated by restriction digestion and Sanger sequencing (Sangon Biotech).

Cell lines

All cell lines were obtained from the American Type Culture Collection (ATCC) and authenticated by short tandem repeat (STR) profiling within the last 6 months prior to experimentation. The human T cell cancer cell line Jurkat E6-1 and mouse T cell cancer cell lines EL-4, as well as the mouse colon cancer cell line MC38 and lung cancer cell line TC-1, were cultured in RPMI-1640 medium (Gibco) supplemented with 10% heat-inactivated fetal bovine serum (FBS, Gibco), 100 U/ml penicillin (Sangon Biotech), and 100 U/ml streptomycin (Sangon Biotech). The cells were maintained in a humidified incubator at 37 °C with 5% CO_2. The HEK293T cell line (catalog no. CRL-1573) and B16 cell line were also obtained from the ATCC. HEK293T cells were cultured in Dulbecco's Modified

Eagle Medium (DMEM, Gibco, catalog no. 11965092) supplemented with 10% heat-inactivated FBS, 100 U/ml penicillin-streptomycin (Gibco, catalog no. 15140122). B16 cells were cultured in the same DMEM medium with the same supplements. Both cell lines were incubated at 37 °C in a 5% CO_2 humidified incubator. Cells were passaged when they reached 70-80% confluence using 0.05% trypsin-EDTA (Gibco, catalog no. 25300054) for detachment.

Lentivirus packaging and transduction

HEK293T packaging cells were seeded at a density of 3×106 cells per 10-cm dish in Dulbecco's Modified Eagle's Medium (DMEM, Thermo Fisher Scientific) supplemented with 10% fetal bovine serum (FBS, Sigma-Aldrich) and 1% penicillin-streptomycin (Thermo Fisher Scientific), and incubated at 37℃in a humidified atmosphere with 5% CO2. Transfection was carried out using Lipofectamine 2000 Reagent (Thermo Fisher Scientific) following the manufacturer's protocol: a mixture of 3 μg of OSA-expressing plasmids and 9 μg of lentiviral packaging plasmids (pMD2.G for envelope and Pax2-1 for packaging components, from Addgene), with total DNA adjusted to 12 μg, was incubated at room temperature for 20 min and added drop-by-drop to the cells. Forty-eight hours post-transfection, supernatants with lentiviral vectors were harvested, filtered through a 0.45-μm filter (Millipore), and concentrated with a 10% sucrose solution by ultracentrifugation at 10,000g for 4 h at 4℃ in a Beckman Coulter SW32Ti rotor. Virus preparations were titrated using HEK293T cells as targets: serial dilutions were added to HEK293T cell cultures, and 72 h later, the number of transduced cells was determined by detecting GFP expression (if present) via flow cytometry. For Jurkat cell transduction, Jurkat cells were seeded at a density of 2×106 cells per well in 6-well plates in RPMI-1640 medium (Thermo Fisher Scientific) with 10% FBS and 1% penicillin-streptomycin, and concentrated lentiviral vectors were added at a multiplicity of infection (MOI) of 5; 48 h later, 1 μg/ml puromycin (Sigma-Aldrich) was added for two-week selection. All procedures were performed in a biosafety level 2 (BSL-2) laboratory following standard safety protocols for handling lentiviral vectors.

ELISA analysis

Cytokine secretion profiles of interleukin-2 (IL-2), interferon-γ (IFN-γ), and tumor necrosis factor-α (TNF-α) from human primary T cells, Jurkat cells, murine T cells, and EL-4 cells were quantified using sandwich ELISA kits. The kits used were from Thermo Fisher Scientific: for human samples, IL-2 (Cat# EH2IL2), IFN-γ (Cat# EHIFNG), TNF-α (Cat# EHTNFA); for mouse samples, IL-2 (Cat# EMIL2), IFN-γ (Cat# EMIFNG). For the analysis of serum IL-6 (Beyotime Biotechnology, Cat# PI326), TNF-α (Beyotime Biotechnology, Cat# PT512), hepatic markers alanine aminotransferase (ALT, Abcam, Cat# ab105134) and aspartate aminotransferase (AST, CUSABIO, Cat# CSB-E12649m), and renal biomarkers neutrophil gelatinase-associated lipocalin (NGAL, Bio-Swamp, Cat# ZN2689) and monocyte chemoattractant protein-1 (MCP-1, Lianke Biotech, Cat# EK287HS-96), assays were carried out following the manufacturer-recommended protocols. Absorbance measurements were conducted on a BioTek Synergy H1 microplate reader (Agilent) with dual-wavelength correction at 450 nm/570 nm. Data were normalized to standard curves generated using a 4-parameter logistic fit, with an R^2 value > 0.99.

Identification of intracellular calcium flux

For intracellular calcium flux identification, cells were loaded with Fluo-8 AM (ab142773) (4 mM, 100 ml) in HHBS [Hanks' Balanced Salt Solution with 20 mM Hepes at 37°C under 5% CO_2 for 1 h protected from light, followed by two washes with HHBS. Cells were subsequently stimulated with 1 ug/ml anti-CD3 antibody (SinoBiological,OKT3, GMP-10977) /anti-CD28 antibody (Sino Biological,CD28.2,GMP-11524) alongside various treatments, then analyzed using a fluorescence microplate reader. Timepoint values represent means from three independent central views across triplicate wells. Fluorescence intensity analysis utilized maximum group values (MAX) as baseline, with real-time MFI (Mean Fluorescence Intensity)expressed as percentage change relative to baseline.

Western blots

Jurkat or OSA-Jurkat cells were stimulated with 1 μg/ml of anti-CD3 and/or anti-CD28 antibodies. After 1 hour, the cells were lysed using RIPA lysis buffer containing sodium orthovanadate and a protease inhibitor, incubating on ice for 15 minutes. The lysates were then subjected to high-speed centrifugation to remove debris. Samples were combined with 5× SDS loading buffer and heated at 95°C for 10 minutes. The protein samples were loaded onto gels and electrophoresed at 120 V for 90 minutes. Following this, proteins were transferred to nitrocellulose membranes using transfer buffer at 100 V for 35 minutes. The membranes were blocked with nonfat dry milk for 1 hour and subsequently washed with Tris-buffered saline containing 0.1% Tween-20 (TBST). After three washes with TBST, the membranes were incubated overnight with a primary antibody, followed by a 1-hour incubation with a horseradish peroxidase (HRP)-conjugated secondary antibody at 4°C. The membranes were washed three times with TBST before subjected to chromogenic development using 3,3'-diaminobenzidine (DAB) substrate under optimized exposure conditions (room temperature, protected from light), with the reaction terminated by rinsing in distilled water to prevent overdevelopment. The antibodies utilized in this experiment included GAPDH (Proteintech, 10494-1-AP), NF-κB (p65) (Abcam, ab28856), and AP-1 (JUN-C) (Abbkine, ABP50261).

RNA-seq Analysis of OSA-Jurkat Cells

Total RNA from OSA-Jurkat cells was isolated using Trizol Reagent. After assessing its quality with a NanoDrop spectrophotometer, 3 μg of RNA was used to synthesize cDNA with the SMARTer Ultra Low Input RNA Kit.Sequencing libraries were prepared using the Nextera XT kit (Illumina). The process included mRNA purification, fragmentation, cDNA synthesis in two steps, end-modification, adapter ligation, size-selection (400-500 bp) with the AMPure XP system, and PCR enrichment (15 cycles). The libraries were quantified using the Agilent high-sensitivity DNA assay on a Bioanalyzer 2100 system. Sequencing was carried out on a P3 flowcell-NextSeq2000 platform. Raw sequencing data was processed with fastp(0.22.0) to obtain clean reads, which were then mapped to the reference genome using HISAT2 (v2.1.0). Gene expression was analyzed by HTSeq (v0.9.1) and normalized with FPKM/TPM[34]. Differential gene expression was determined by DESeq2 (v1.38.3) with criteria of ｜log2FoldChange｜>1 and P−value<0.05. All analyses were performed on the Personalbio Genes Cloud platform.

CRISPR–Cas9 knockin

CRISPR-Cas9-mediated knockin was performed using a modified approach based on previously published methods (HITI reference). Briefly, A single-guide RNA (sgRNA) targeting the CD3Z locus (guidesequence: *5'-TTTCACCGCGGCCATCCTGC-3'*) was designed and cloned into the BbsI restriction site of the PX330 vector (Addgene #42230) via Gibson assembly. The donor sequences, synthesized by Genewiz, were subsequently cloned into the P-EASY plasmid. A total of 10 μg of Cas9 protein and 10 μg of donor DNA were used for electroporation of 2 million T cells using the preset DS104 program of the 4D-Nucleofector™ system (Lonza). Electroporation was conducted according to the manufacturer's instructions.After electroporation, cells were resuspended in pre-warmed RPMI-1640 medium containing 10% FBS.

Primary human T cellisolation, activation and expansion

Whole blood obtained from healthy donors (BER-YXY-2024023) PBMCs were isolated from whole blood using density gradient centrifugation with Ficoll-Paque PREMIUM (1.077 g/mL)[35]. Briefly, blood was diluted 1:2 with saline, layered over separation medium, and centrifuged at 750 × g for 15 min (brake disabled). The PBMC layer was collected, washed twice in PBS, and centrifuged at 200 × g for 5 min. Autologous plasma was heat-inactivated (56°C, 30 min) and stored at 4°C for subsequent use. CD3+ T cells were isolated via magnetic-activated cell sorting (MACS) using CD3 MicroBeads (MiltenyiBiotec). Cells were incubated with CD3 MicroBeads (20 μL per 1×10^7 cells) in

sorting buffer (DPBS + 0.5% BSA + 2 mM EDTA) at 4°C for 15 min, washed, and passed through a pre-rinsed LS column. The CD3+ fraction was eluted after removing unbound cells. For activation and expansion, CD3 antibodies (5 μg/mL) were immobilized on 6-well plates overnight. Purified T cells were cultured in RPMI-1640 medium supplemented with 10% FBS, CD28 antibody (3 μg/mL), and IL-2 (200 IU/mL) at 2.5×10^5 cells/mL. Cultures were maintained in a 5% CO_2 incubator for 2–5days, achieving 3–10-fold expansion. The purity and activation status of T cells were evaluated by flow cytometry.

Flow cytometry analysis

Flow cytometry was utilized to assess the efficiency of gene editing or gene introduction mediated by the OSAT molecule. $CD3^+$ T cells harvested at distinct time points were stained with fluorescently-conjugated antibodies specific for human CD25 (PE, Miltenyi), human CD69 (APC, Milteny), mouse anti-CD3 (FITC, Miltenyi), mouse anti-PD-1 (VioBlue, Miltenyi), mouse anti-TIM-3 (PE, Miltenyi,), and mouse anti-LAG-3 (APC, Miltenyi,), followed by flow cytometric analysis. All data were processed using FlowJo software.

T-cell Cytotoxicity Assay

T cells and target cells were counted and mixed in a 1:1 ratio, with 2 x 10^5 cells added to each well of a 24-well plate. After a 24-hour co-culture period, the cells were harvested and washed three times with flow cytometry staining buffer. The samples were subsequently stained with Annexin V-APC and DAPI (Elabscience, E-CK-A258) for 15 minutes at room temperature. FlowJo V10 software was utilized for data analysis. The T cell-mediated killing rate (%) was determined by calculating the percentage of Annexin V-positive cells among the tumor cells (FITC+) co-cultured with T cells, subtracting the percentage of Annexin V-positive tumor cells cultured alone. The formula for the T cell-killing rate is as follows: T cell-killing rate (%) = Annexin V positive rate (%) of tumor cells co-cultured with T cells-Annexin V positive rate (%) of tumor cells cultured alone. The assessment of Annexin V positivity was conducted in accordance with established methodologies[36].

Mice

Female C57BL/6 mice, 6-9 weeks old, were obtained from Charles River Laboratory (Beijing, China) and randomly allocated to either the experimental or control group. Mice were housed in specific pathogen-free animal facilities at the Hebei University of Engineering, maintained on a 12-h light–dark cycle. The housing temperature was controlled within a range of 21-24 °C, and relative humidity was maintained between 25% and 61%. Mice were provided with diet [specify diet number if available]. All animal experiments were carried out in strict accordance with the guidelines and regulations of the Hebei University of Engineering Animal Care and Use Committee, Hebei, China.

Tumor models

In the present study, female C57BL/6 mice aged 6-8 weeks were selected. The mice were first shaved, and then underwent subcutaneous injection. For the injection of tumor cells, three types of cells were used: B16 cells at a density of $2x10^5$ cells per 0.2 ml per mouse, MC38 cells at $5x10^5$ cells per 0.2 ml per mouse, and TC-1 cells at $5x10^5$ cells per 0.2 ml per mouse.During the experimental process, the tumor volumes were regularly evaluated. Specifically, the size of the tumor was measured in two dimensions using a digital caliper every 2-3 days. The tumor volume was calculated by the formula: Volume = (length x $width^2$)/2. In some experiments, such as those related to anti-tumor efficacy, if the tumor reached 15 mm in its longest axis, or developed ulceration or necrosis, it was considered as an endpoint, similar to the definition in previous studies. Additionally, for certain experimental setups like rechallenge experiments, if required, tumor cells could be injected subcutaneously on the opposite flank of the mice.

Mouse CD3+ T-cell isolation

Tumors were excised 12-18 days post tumor engraftment. Fresh tumor tissues were carefully washed with appropriate buffer solutions and then cut into approximately 1 mm^3 pieces. To facilitate

tissue dissociation, the samples were incubated with a mixture of DNase, collagenase (such as collagenase IV at a concentration of 1 mg ml^{-1}), and hyaluronidase. This digestion process was carried out at 37 °C in a shaking incubator set at 200 r.p.m. for 30 minutes. After digestion, the cell suspension was filtered through a 70-μM cell strainer to remove large debris. Subsequently, density gradient centrifugation, for example, using Percoll, was performed to separate lymphocytes. The white cell layer, which is enriched with TILs and located between 75% and 100% separation liquid layers, was carefully collected. For the isolation of CD3+ T cells, positive selection was carried out using mouse CD4/CD8 (TIL) MicroBeads (MiltenyiBiotec), following the detailed manufacturer's instructions precisely. When isolating CD3+ T cells from peripheral blood mononuclear cells (PBMCs), density gradient centrifugation was first used to separate lymphocytes. Then, CD3+ T cells were isolated from the white cells using the same mouse CD4/CD8 (TIL) MicroBeads according to the manufacturer's protocol. The purified CD3+ T cells were amplified in RPMI-1640 medium supplemented with 10% fetal bovine serum (FBS) and a high dose of mouse interleukin-2 (IL-2, 100 units/mL; eBioscience).

CCK8 assay

The effector cells include TILs and OSAT, and the corresponding tumor cell lines were used as target cells. A 96-well plate was prepared with a control well containing RPIM-1640 complete medium supplemented with 10% FBS, and experimental and control wells. Subsequently, 100 μl of target cells (2×104/ml) and 100 μl of effector cells (1× 105/ml, 2×105/ml, 4×105/ml) were added to the experimental wells. The plate was then incubated at 37℃ with 5% CO2 for 24 hours. Afterward, 20 μl of CCK8 solution was added to each well. Following a 4-hour incubation, the anti-tumor activity of TILs in vitro was assessed using the CCK8method according to manufacturer's instruction(MCE).

In vivo murine tumor experiments

To assess the in vivo anti-tumor activity of OSAT compared to traditional TIL, we conducted experiments using three tumor models over two time periods. In the first period, tumor tissue was removed, and CD3+ TIL cells were extracted 12-18 days after tumor formation. After amplification with IL2, half of the TIL cells were introduced to the OSA plasmid through electroporation, referred to as OSAT, while the remaining half remained as traditional TIL (n-TIL). These cells were then injected back into the tumor model mice via tail vein injection (2x107 cells/mice). Anti-PD-1 antibody (clone RMP1-14, BioXcell) was injected intraperitoneally in the corresponding groups at day 12,15,18,21after tumor cell inoculation. Tumor volume was measured every three days using a Vernier caliper, and survival time was recorded. Tumor volume was calculated using the formula: volume = (length × width2)/2.

Statistical Analysis

Statistical analysis was performed using GraphPad Prism software（10.3.1）. Data are presented as mean ± standard deviation unless otherwise stated. Statistical tests included one-way or two-way ANOVA with tukey's multiple comparisons test and log-rank (Mantel-Cox) test. Differences were considered statistically significant when $P < 0.05$. All statistical tests were two-sided, and sample sizes were determined based on prior experience and power analysis to ensure sufficient statistical power to detect meaningful differences.

Data availability

Transcriptome data have been deposited in the NCBI Sequence Read Archive(BioProject ID：PRJNA1237508). All other data are available in the maintext or the Supplementary Information. Source data are provided withthis paper.

References

34. Gibson, D. G. et al. Enzymatic assembly of DNA molecules up to several hundred kilobases. Nat. Methods 6, 343–345 (2009).
35. Li, Y. et al. Magnetic-activated cell sorting in translational immunology: A consensus statement on technical optimization and quality control. *Nat. Protoc.* **18**, 2133–2157 (2023)
36. Zhao, X., et al. Tuning T cell receptor sensitivity through catch bond engineering. Science 376, eabl5282 (2022)

Acknowledgements

This work was supported by the Key Research and Development Program of Hebei Province (Grant No. 22372402D; Grant No.21372902D). Natural Science Foundation of China (Grant No. 82374090; Grant No. U21A20415). Hebei Natural Science Foundation (Grant No. H2024402005). We thank the facility support of Gene Editing Research Center, Hebei University of Science and Technology.

Author Contributions

Yongqiang Wu and Xueshuai Ye conceived the project, designed all experiments. Yongqiang Wu, Xueshuai Ye, Yufeng Zhu, Shengchao Liu and Jiabao Song performed the experiments. Yongqiang Wu, Xueshuai Ye, QichenY uan, Dejing Kong and Lianmei Zhao analyzed the data. Yongqiang Wu and Lianmei Zhao wrote the manuscript with help from all authors.

Competing interests

The authors declare that they have no financial or non-financial competinginterests.

Extended Data

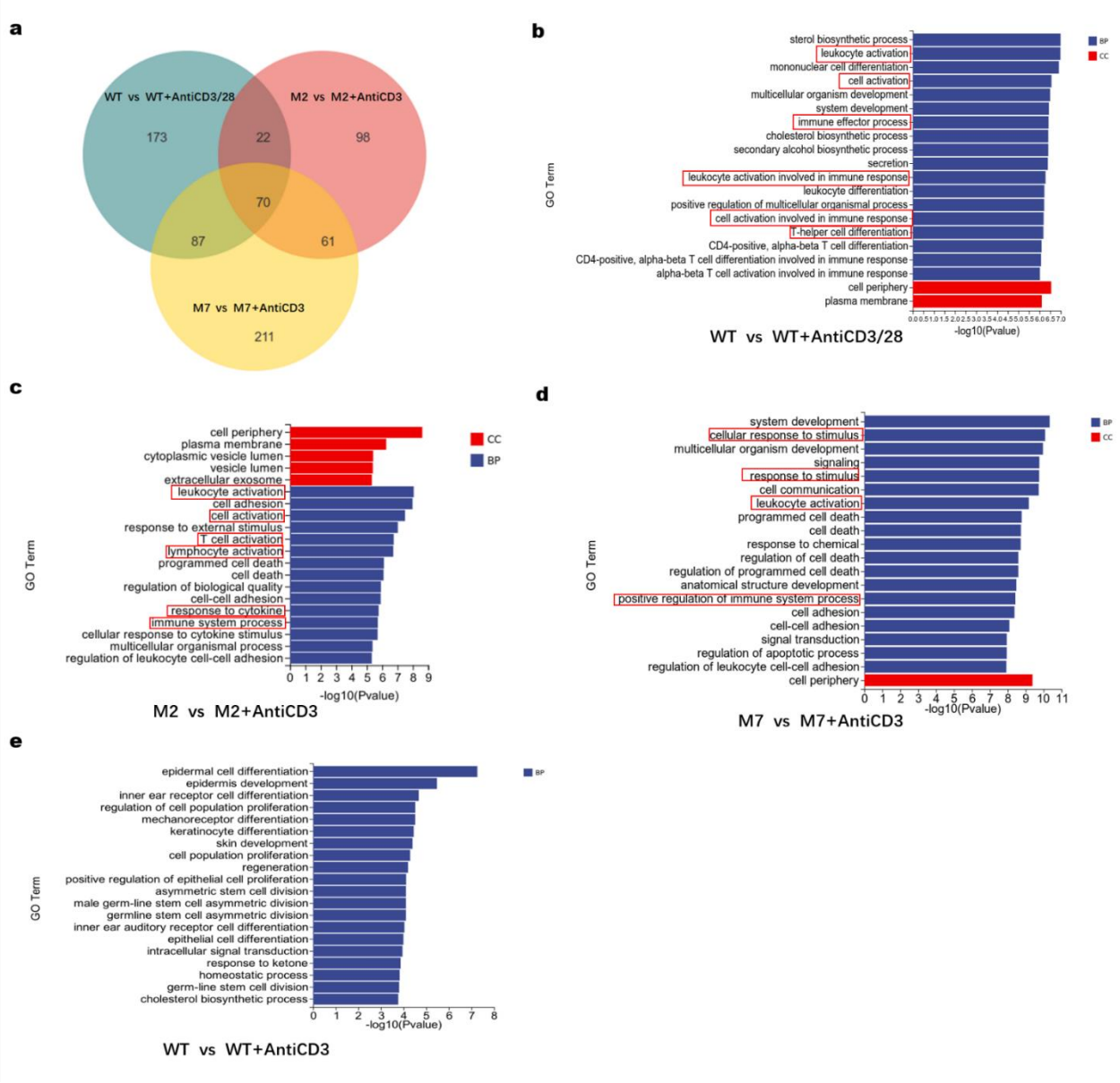

Extended Data Fig. 1 | Transcriptomic profiling validated functional equivalence between OSA-Jurkat and dual-stimulated wild-type (WT) Jurkat cells.
(a) Venn diagram of differentially expressed genes. **(b-e)** Gene Ontology (GO) enrichment analysis comparing WT vs. WT+AntiCD3/28, M2 vs. M2+AntiCD3, M7 vs. M7+AntiCD3, and WT vs. WT+AntiCD3 Jurkat cells. The top 20 most significantly enriched GO terms for differentially expressed genes are shown. GO enrichment analysis was performed using the clusterProfiler R package. Differentially expressed genes were annotated to GO terms, and enrichment was calculated via hypergeometric distribution. Statistical significance was defined by a P-value threshold of <0.05, identifying GO terms overrepresented in differential gene sets relative to the genomic background. This analysis characterized the primary biological functions associated with differentially expressed genes.

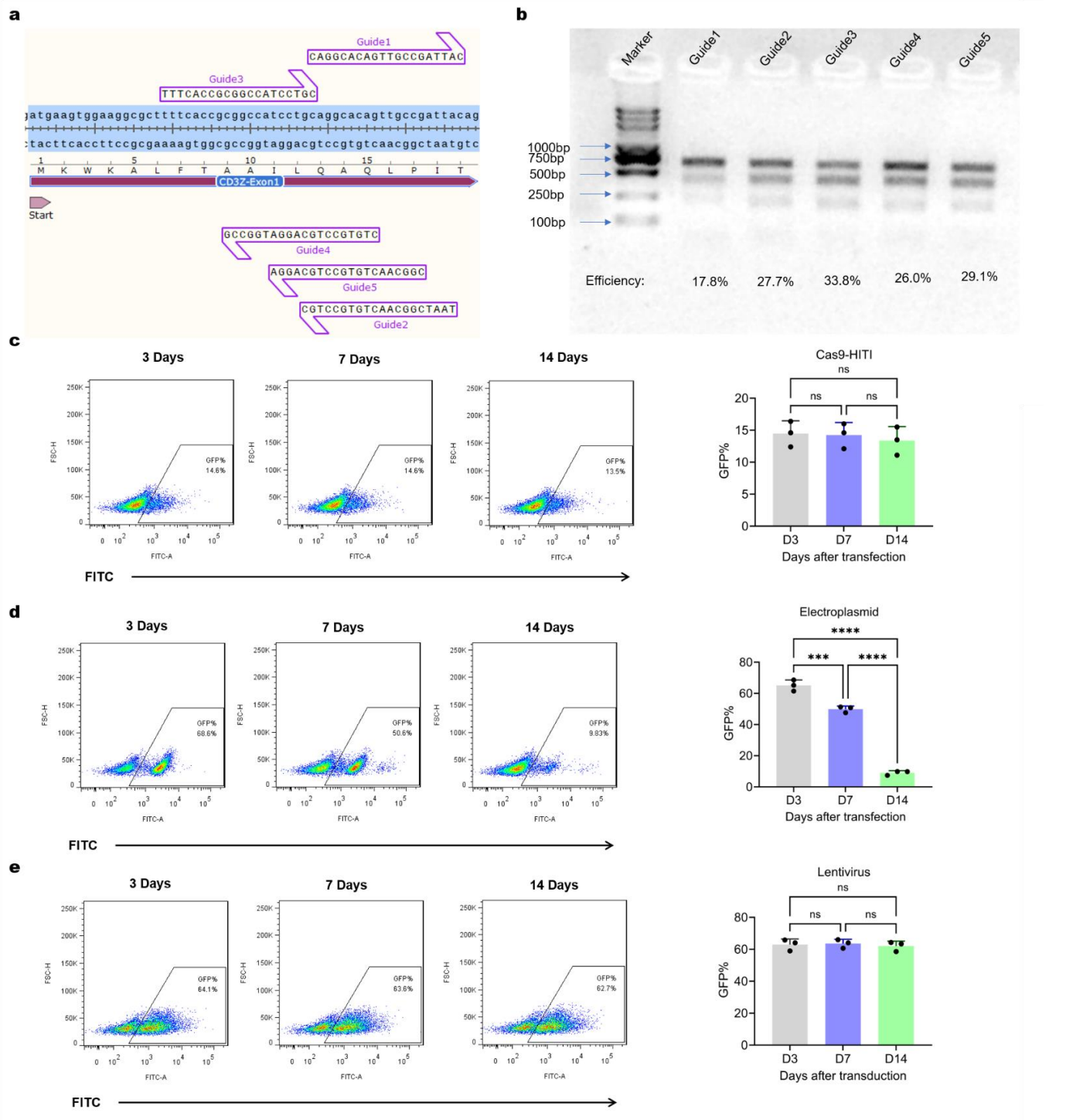

Extended Data Fig. 2 | Design and characterization of Cas9-HIHI genome editing via T7E1 assay and replicable plasmid maps with expression persistence.
(a) Schematic representation of the genomic locations of the five single-guide RNAs (sgRNAs) targeting the *CD3Z* gene. **(b)** Detection of indels at the *CD3Z* exon 1 locus using Cas9-sgRNA complexes with five different guides. PCR amplification was performed using primers CD3Z-F (GCGAATTTCTTGGCCCTGTC) and CD3Z-R (GTTTCTCTACCCTGGGCCTG). Annealed PCR products were digested with T7 Endonuclease I (New England Biolabs) for 30 min, resolved by 1.5% agarose gel electrophoresis, and quantified by band intensity analysis. Indel efficiency was calculated using ImageJ software via the formula: $100 \times [1 - \sqrt{(1 - (b + c)/(a + b + c))}]$, where *a* denotes the integrated intensity of the undigested PCR fragment and *b*/*c* represent the intensities of cleavage products. **(c-e)** Persistence of plasmid expression following Cas9-HITI,electroplasmid and lentivirus. Error bars represent mean ± SEM. Statistical significance

was determined by one-way ANOVA with tukey's multiple comparisons test (*P < 0.05, **P < 0.01, ***P < 0.001, ****P <0.0001; ns = not significant).

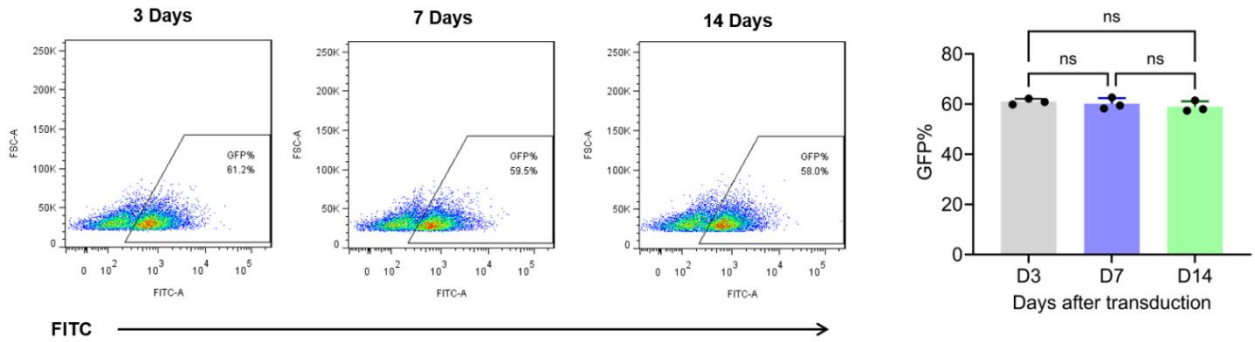

Extended Data Fig. 3 | Duration of OSAT molecule expression in murine cells delivered by lentivirus.

Efficiency and persistent expression of OSAT molecules delivered into the EL-4 murine T cell line via lentiviral infection.Error bars represent mean ± SEM.Statistical significance was determined by one-way ANOVA with tukey's multiple comparisons test (*P < 0.05, **P < 0.01, ***P < 0.001, ****P <0.0001; ns = not significant).

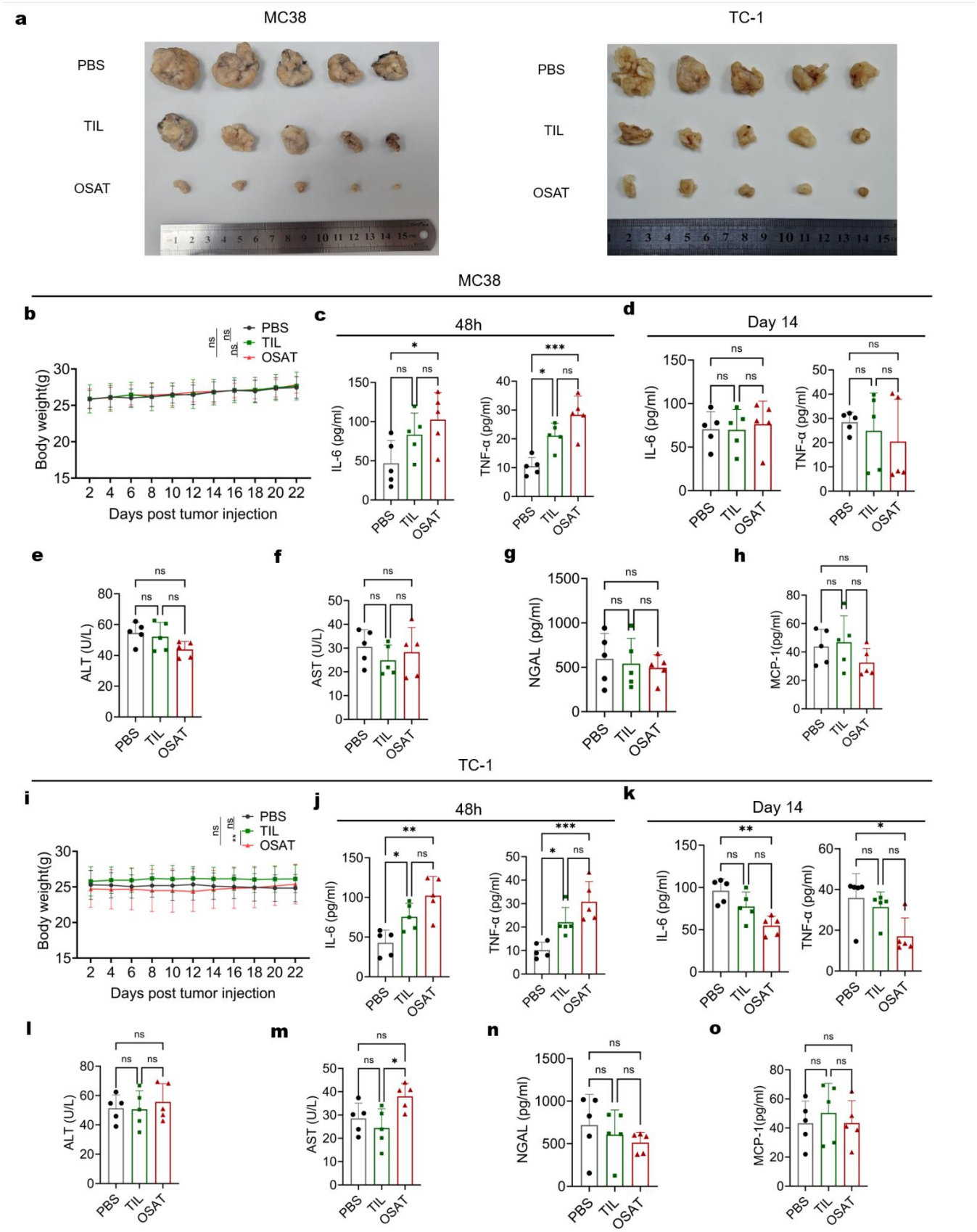

Extended Data Fig. 4 |In vivo anti-tumor efficacy evaluation of OSAT in MC38 and TC-1 models

(a) Representative macroscopic images of excised MC38 or TC-1 tumors across treatment groups at endpoint (tumors harvested on Day 21 post-inoculation; n = 5). **(b)** Body weight changes in MC38 tumor-bearing mice across treatment groups (time-matched with tumor growth monitoring). **(c-d)** ELISA analysis of the cytokine production of IL-6 and TNF-α in the sera of MC38 model mice

that subjected to the indicated treatment after 48hours or 14days.Statistical analysis was performed using non-parametric tests. **(e-h)** Serum biomarkers of hepatic/kidney toxicity (ALT, AST) and inflammation (NGAL, MCP-1) at Day 14 post-treatment in the MC38 model.(i)Body weight changes in TC-1 tumor-bearing mice across treatment groups (time-matched with tumor growth monitoring). **(j-k)** ELISA analysis of the cytokine production ofIL-6 and TNF-α in the sera of TC-1 model mice that subjected to the indicated treatment after 48hours or 14days.Statistical analysis was performed using non-parametric tests. **(l-o)** Serum biomarkers of hepatic toxicity (ALT, AST) and kidney toxicity (NGAL, MCP-1) at Day 14 post-treatment in the TC-1 model. The error bars indicate the mean ± the standard error of the mean. Statistical significance was determined by one-way or two-way ANOVA with tukey's multiple comparisons test (*P < 0.05, **P < 0.01, ***P < 0.001, ****P <0.0001; ns = not significant).

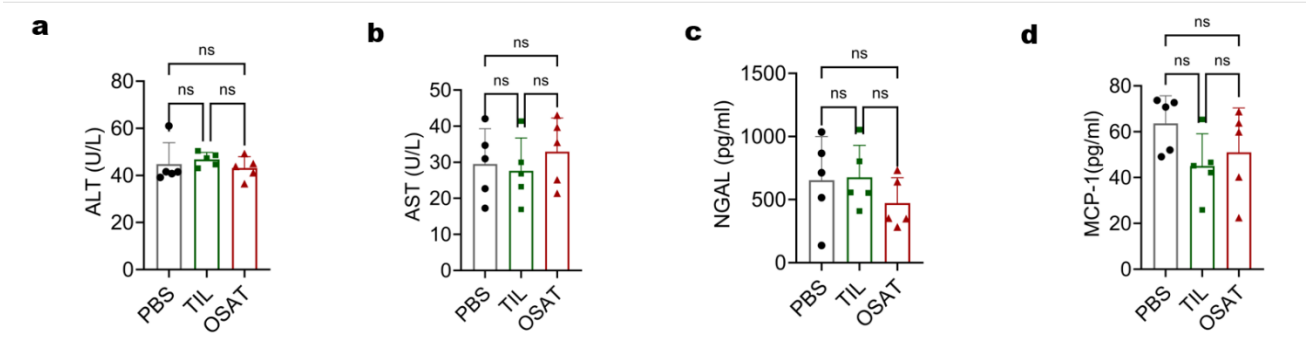

Extended Data Fig. 5 | Hepatic and renal safety biomarkers following combination with PD-1 blockade

(a-d) Serum biomarkers of hepatic toxicity (ALT, AST) and renal toxicity (NGAL, MCP-1) in the TC-1 model at day 14 post-treatment. Error bars represent mean ± SEM. Statistical significance was determined by one-way ANOVA with tukey's multiple comparisons test (*P < 0.05, **P < 0.01, ***P < 0.001, ****P <0.0001; ns = not significant).